ACS OMEGA

http://pubs.acs.org/journal/acsodf

Article

Therapeutic Potential of Methotrexate-Loaded Superparamagnetic Iron Oxide Nanoparticles Coated with Poly(lactic-*co*-glycolic acid) and Polyethylene Glycol against Breast Cancer: Development, Characterization, and Comprehensive In Vitro Investigation

Sankha Bhattacharya,* Bhupendra G Prajapati, Nemat Ali,* Mohamed Mohany, Mourad A. M. Aboul-Soud, and Rehan Khan

Cite This: *ACS Omega* 2023, 8, 27634−27649

Read Online

ACCESS | Metrics & More | Article Recommendations

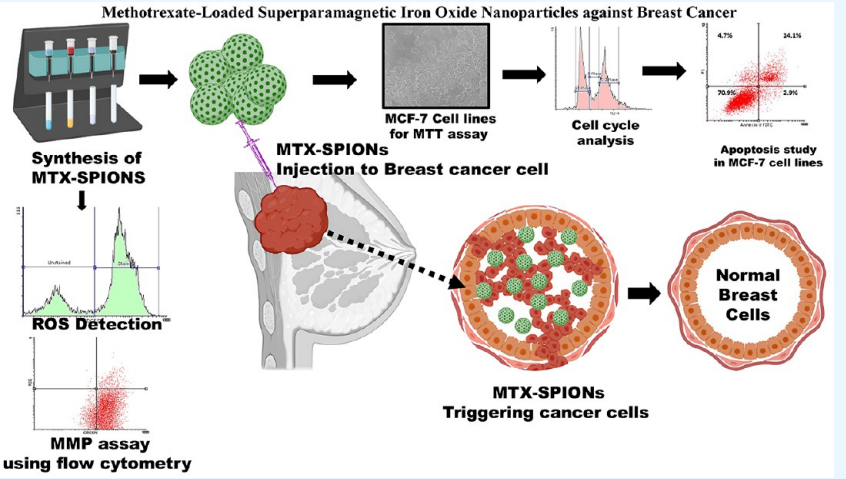

ABSTRACT: Novel superparamagnetic iron oxide nanoparticles (SPIONs) of Methotrexate (MTX) were developed using supercritical liquid technology and optimized with a Box−Behnken design in order to assess its potential as a candidate for the treatment of breast cancer. MTX-SPIONs coated with poly(lactic-*co*-glycolic acid)−polyethylene glycol 400 had an aggregate size of 500 nm and an encapsulation efficiency of 46.8 ± 3.9%. The Fourier-transformed infrared spectroscopy analysis revealed a shift in the main bands due to intermolecular hydrogen bonds, whereas the differential scanning calorimetry analysis revealed the absence of the MTX melting endotherm, indicating complete encapsulation with oxide nanoparticles. The zeta potential results indicated a value of 4.98 mV, whereas the in vitro release study revealed an initial burst release followed by a considerable release of 35.1 ± 2.78% after 12 h. Using flow cytometry, control, MTX, and MTX-SPIONs were evaluated for apoptosis, with MTX-SPIONs exhibiting greater apoptosis than the control group and MTX. In addition, MTX-SPIONs inhibited cell division and content organization while substantially increasing the proportion of cells in the G1 and G2 phases relative to the control group. MTX-SPIONs exhibited prolonged anticancer effects against MCF-7 cell lines compared to MTX alone, indicating that SPION-delivered chemotherapeutics may increase cytotoxicity. The medication was stable with low encapsulated drug loss, suggesting that the supercritical liquid technology-based method is a promising way for generating drug−polymer magnetic composite nanoparticles for cancer treatment.

INTRODUCTION

Cancer is the unwanted growth of the body's cells that multiplies faster than healthy cells.[1] It has been reported that breast cancer is the second most common cancer in women worldwide, and many cases of death have been reported.[2] Various treatments have been reported for the treatment of cancer cells, such as surgery, radiation, chemotherapy, and

Received: May 17, 2023
Accepted: July 11, 2023
Published: July 19, 2023

combined therapy.[3] Currently used conventional therapies are chemotherapy, hormonal therapy, and targeted therapy.[4] Although various treatments are available, it is still challenging to treat cancer cells and increase the survival rate. Presently, nanoparticle (NP)-based systems have been developed for the delivery of chemotherapeutic drugs for the treatment of cancer.[5] Nanoparticles are small, ranging from 1 nm to several hundred nanometers, and are building blocks of nanotechnology. Nowadays, they have gained more attention for their application in the treatment of cancer. Methotrexate sodium is an antineoplastic drug that inhibits dihydrofolate reductase, thus preventing the conversion from dihydrofolate to tetrahydrofolate.[6] Methotrexate sodium is used to treat various cancers, such as breast cancer, lung cancer, head and neck cancer, and skin cancer.[7] Apart from its original use as a cancer chemotherapeutic agent, it has been suggested for several other diseases, such as psoriasis, multiple sclerosis, Crohn's disease, and rheumatoid arthritis. Methotrexate acts as a cancer chemotherapeutics agent by inhibiting dihydrofolate reducatase with high affinity, resulting in the depletion of tetrahydrofolates required for the synthesis of purines and thymidylate.[8] Subsequently, the synthesis of DNA and RNA, as well as other metabolic reactions, are interrupted; however, MTX does not act simply as an antiproliferating agent for the cells responsible for the joint inflammations in rheumatoid arthritis.[9] The rapid clinical remission as seen with low-dose MTX administration as well as the rapid flare of the disease after drug discontinuance suggest that the mechanism of action of low-dose MTX might be more anti-inflammatory than antiproliferative. In fact, MTX inhibits both dihydrofolate reducatase and other folate-dependent enzymes and leads to adenosine overproduction, which can induce immunosuppression.

Superparamagnetic iron oxide nanoparticles (SPIONs),[10] the only clinically approved metal oxide NPs, hold immense potential in a wide variety of biomedical applications such as magnetic resonance imaging (MRI), targeted delivery of drugs or genes, tissue engineering, targeted destruction of tumor tissue through hyperthermia, magnetic transfections, iron detection, chelation therapy, and tissue engineering.[11] The SPIO agents have a unique superparamagnetic property that confers advantages such as the generation of heat in alternating magnetic fields or the ability to be guided to a specific tissue or organ by an external magnetic field. This property is therefore central to the exploitation of SPIO in many of those mentioned above in technological and biomedical applications. Based on the hypothesis, the objectives of the investigation were to prepare and evaluate PLGA−PEG-coated superparamagnetic iron oxide nanoparticles (SPIONs) of MTX.

Furthermore, optimization of processing parameters and used excipients in drug delivery fabrication is essential.[12] Several studies reported in the fabrication of NPs adopted the use of an experimental statistical design. An experimental design is the process of carrying out research with an objective in controlled and precise form to maximize the results with specific conclusions. Therefore, the objective of the research was to fabricate polymer-coated SPIONs of MTX for breast cancer targeting that could ultimately reduce the early clearance from the body, minimize nonspecific cell interactions, and increase their internalization efficiency within target cells.

To summarize, the present research aims to undertake the development and optimization of a new category of drug delivery system that employs superparamagnetic iron oxide nanoparticles (SPIONs) for the treatment of breast cancer. The study demonstrated that the SPIONs exhibited favorable encapsulation efficacy, consistent drug release, and improved cytotoxicity in comparison with conventional MTX therapy.

In this study, we employed poly(lactic-*co*-glycolic acid)−poly(ethylene glycol) (PLGA−PEG) polymers for the fabrication of methotrexate superparamagnetic iron oxide nanoparticles (MTX-SPIONs) using supercritical liquid technology. The choice of PLGA−PEG offered several advantageous features, including biocompatibility and biodegradability of PLGA, controlled drug release through modulation of polymer composition and molecular weight, enhanced targeting and prolonged circulation through PEGylation, improved stability of nanoparticles, and efficient encapsulation of hydrophobic drugs like methotrexate. These properties collectively establish PLGA−PEG as an ideal candidate for the development of drug−polymer magnetic composite nanoparticles with potential applications in cancer treatment.

The investigation additionally showcased the prospective application of supercritical liquid technology in the production of drug−polymer magnetic composite nanoparticles. The implications of these findings are significant for the domain of cancer therapy and have the potential to facilitate the advancement of more efficient and precise treatments for individuals with breast cancer. Additional investigation is required to evaluate the clinical practicability and security of this methodology.

MATERIAL AND METHODS

Materials. Methotrexate was obtained as a gift sample from Neon Pharmaceutical (Bangalore, India). Ferric chloride and ferrous chloride were purchased from Central Drug House (P) Ltd., New Delhi, India. Ammonium hydroxide was purchased from HiMedia Laboratories Pvt. Ltd., Mumbai, India. Poly(lactic-*co*-glycolic acid) (PLGA) and Polyethylene glycol 400 (PEG-400) were purchased from Sigma-Aldrich Pvt. Ltd. HPLC-grade acetonitrile was purchased from Loba Chemie (Mumbai, India). The dialysis membrane was purchased from HiMedia Laboratories Pvt. Ltd. All other chemicals and reagents were of analytical grade reagent.

METHODS

Preformulation, Physical Appearance, and Calibration Curve of Methotrexate. Methotrexate was evaluated for its physical appearance, melting point, and solubility. Briefly, the physical appearance of MTX was quantified by visual observation for color, odor, and appearance. The melting point was quantified using a capillary melting point apparatus (ANALAB ThermoCal25+, India). The maximum absorbance of MTX was measured by using a UV−vis spectrophotometer (Shimadzu 1700, Japan). In brief, 10 mg of MTX was dissolved in sodium bicarbonate (10% v/v) and measured at wavelengths of 200 to 400 nm using a UV−vis spectrophotometer. Moreover, the calibration curve of MTX was further measured using an HPLC (Waters 2489) equipped with a UV detector and reversed-phase column (ODS 5 μm, 4.6 mm × 250 mm, Waters Sunfire). The mobile phase is composed of acetonitrile and buffer in a ratio of 65:35 and a flow rate of 1 mL/min with a column temperature of 26.7 °C. Briefly, 10 mg of MTX was dissolved in sodium bicarbonate (10% v/v) to produce a stock

https://doi.org/10.1021/acsomega.3c03430
ACS Omega 2023, 8, 27634−27649

Table 1. Screening for Process Parameter and Material Attribute

S. No.	Ammonium hydroxide concentration (%)	Stirring time (h)	Stirring speed (RPM)	Particle size (nm)	PDI
1	9.95	8	1000	922 ± 20.67	0.39 ± 0.04
2	9.95	8	1000	890.2 ± 20.89	0.33 ± 0.03
3	9.95	8	1000	860 ± 40.67	0.25 ± 0.03
4	9.95	8	1000	840 ± 60.37	0.34 ± 0.01
5	3.3	12	1000	916 ± 30.27	0.27 ± 0.03
6	9.95	12	1200	957 ± 11.67	0.37 ± 0.05
7	9.95	8	1000	1105 ± 34.89	0.27 ± 0.06
8	9.95	4	1200	913.3 ± 25.78	0.39 ± 0.04
9	9.95	8	1000	1103.7 ± 56.78	0.18 ± 0.05
10	9.95	8	1000	997 ± 88.89	0.34 ± 0.05
11	9.95	4	800	779.2 ± 67.23	0.26 ± 0.06
12	9.95	8	1000	923 ± 24.89	0.27 ± 0.04
13	9.95	12	800	987 ± 12.78	0.16 ± 0.08
14	9.95	8	1000	1012.3 ± 23.89	0.15 ± 0.02
15	9.95	8	1000	826.3 ± 18.78	0.26 ± 0.07
16	9.95	8	1000	907 ± 34.82	0.33 ± 0.09
17	16.6	12	1000	779 ± 14.89	0.31 ± 0.04
18	16.6	8	1200	526.2 ± 35.78	0.25 ± 0.04
19	9.95	8	1000	623.5 ± 33.78	0.18 ± 0.04
20	9.95	8	1000	873 ± 67.78	0.35 ± 0.07
21	9.95	8	1000	913 ± 56.67	0.38 ± 0.05
22	9.95	8	1000	786.6 ± 34.89	0.26 ± 0.05
23	9.95	8	1000	554 ± 90.37	0.15 ± 0.08
24	16.6	8	800	485 ± 34.67	0.29 ± 0.05
25	3.3	8	1200	361.8 ± 45.78	0.31 ± 0.06
26	3.3	4	1000	526 ± 27.78	0.37 ± 0.04
27	9.95	8	1000	578.2 ± 22.78	0.18 ± 0.05
28	3.3	8	800	623.9 ± 18.67	0.27 ± 0.08
29	9.95	8	1000	539 ± 36.67	0.34 ± 0.04
30	9.95	8	1000	512 ± 32.89	0.35 ± 0.04
31	16.6	4	1000	369.4 ± 22.78	0.24 ± 0.08
32	9.95	8	1000	214.6 ± 28.89	0.29 ± 0.01
33	9.95	8	1000	302.6 ± 34.78	0.21 ± 0.05
34	9.95	8	1000	426.8 ± 25.78	0.18 ± 0.09
35	9.95	8	1000	585 ± 36.67	0.39 ± 0.03

solution of 1000 μg/mL. The diluted volume of stock solution (50, 100, 150, 200, 250, 300 μg/mL) was filtered using a nylon membrane filter (0.2 μm) and injected in triplicate; peaks were recorded at λ_{max} = 303 nm. Further, the partition coefficient of MTX was quantified in an *n*-octanol:water system. Concisely, a mixture of *n*-octanol and water (1:1 v/v) was equilibrated for 24 h in a separating funnel. Then, 10 mg of MTX was admixed in it, and after 2 h, the quantity of MTX dissolved in both phases was measured using HPLC at 303 nm. Furthermore, the solubility of MTX was computed in various solvents, including water, chloroform, diethyl ether, and sodium bicarbonate, using HPLC at 303 nm.

MTX's structural and functional quantification was measured using Fourier-transformed infrared spectroscopy (FTIR) equipped with Nicolet Omnic Software and differential scanning calorimetry (DSC: Netzsch Instrument 200F3). FTIR spectra of MTX were tested using the KBr disk method in the wavenumber region of 500 to 4000 cm^{-1}, whereas the DSC of MTX was analyzed using a perforated aluminum pan with a scan rate of 10 °C under nitrogen gas (50 mL/s).

Optimization of Ingredients for the Synthesis of SPIONs. The concentration of ammonium hydroxide, stirring speed, and stirring time were optimized on the basis of particle size and the polydispersity index (PDI). The concentration of ammonium hydroxide was used in the range of 3.3 to 16.6%, and the stirring time ranged from 4 to 12 h (Table 1).

Optimization of Variables Using Experimental Design. A Box−Behnken experimental design for response surface methodology was applied to optimize the experimental variable in the fabrication of superparamagnetic magnetite (Fe_3O_4) NPs. An experimental design is a collection of statistical and mathematical techniques useful for modeling and analyzing problems in which several variables influence the response of interest. Moreover, it is an empirical technique developed for analyzing and studying the relationship between a set of controlled experimental factors and observed results.[13] To explain this process mutually with response to Y that depends on the input factors X_1, X_2, ..., X_n, the correlation between the response and the input process parameters are described as $Y = f(X_1, X_2, ..., X_n) + \varepsilon$, where f is the response function, and ε is the error. Since the correlation between the response and input variables is described as a surface of the X_1 and X_2 coordinates in the graphical sense, the response surface study is named. In this design, three independent factors were evaluated, each at three levels, and experimental trials were performed for all 13 possible combinations. The ammonium hydroxide concentration (X_1), stirring time (X_2), and stirring speed (X_3) were selected as independent variables, and

https://doi.org/10.1021/acsomega.3c03430
ACS Omega 2023, 8, 27634−27649

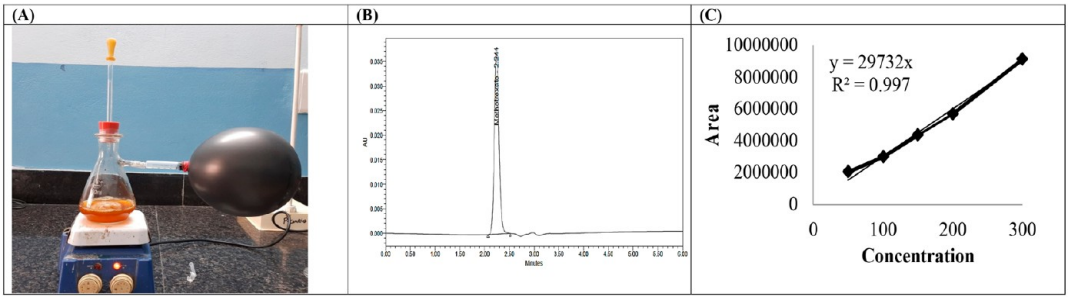

Figure 1. (A) Synthesis of superparamagnetic iron oxide nanoparticles (SPIONs) in the presence of an inert nitrogen environment. (B) HPLC chromatogram of methotrexate. (C) Calibration curve of methotrexate using HPLC.

strength, particle size (Y_1), and PDI (Y_2) were determined as the response variables.

Fabrication of Superparamagnetic Nanoparticles. Superparamagnetic magnetite (Fe_3O_4) nanoparticles were prepared using an improved chemical coprecipitation.[14] Concisely, 3.1736 g of $FeCl_2{\cdot}4H2O$ (0.016 mol) and 7.5684 g of $FeCl_3{\cdot}6H_2O$ (0.028 mol) were dissolved in 320 mL of deionized water, such that Fe^{2+}/Fe^{3+} = 1/1.75. Subsequently, ammonium hydroxide was added to the mixture in the presence of nitrogen gas with vigorous stirring (Figure 1A). The precipitated particles were washed thoroughly with hot water and separated by magnetic decantation. Finally, the magnetic NPs were dried using a lyophilizer (Virtis Genesis SQ EL-85 Lyophilizer, SP Scientific, USA). The lyophilized NPs were stored at 4 °C until further analysis. Furthermore, nanoparticles' hydrodynamic particle size and size polydispersity were assessed using a dynamic light scattering method (Delsa TN Nano C, Beckman colter).

Preparation of PLGAPEG-Coated Superparamagnetic Iron Oxide Nanoparticle. Synthesized SPIONs (15 mg) were suspended in 3 mL of acetone, and 1 mg of MTX was dissolved in DMSO (100 μL). A total of 16 mg of PLGA and PEG 400 were dissolved in acetone (1 mL) separately. Thereafter, MTX was mixed with a polymeric solution over a magnetic stirrer at 1000 rpm (IKA C-MAG HS 7 Magnetic Stirrer, IKA Works, Germany). This polymeric MTX solution was admixed with the SPIONs solution dropwise under stirring using a needle, and the final mixture was dried using a lyophilizer (Virtis Genesis SQ EL-85 Lyophilizer, SP Scientific, USA).

Characterization of PLGA−PEG-Coated Superparamagnetic Iron Oxide Nanoparticle. *Particle Size, Zeta Potential, and Morphology.* The hydrodynamic particle size and size polydispersity of nanoparticles were assessed using a dynamic light scattering method (Delsa TN Nano C, Beckman coulter, USA). The zeta potential of the NPs was measured in KCl (1 mM) using Delsa Nano C at 25 °C (Delsa TN Nano C, Beckman coulter, USA). The surface morphology of the NPs was observed by SEM (FEI Quanta SEM, Thermo Fisher Scientific, USA). The morphology of the particles was achieved using transmission electron microscopy (TEM) (JEOL JEM-1400Plus TEM, JEOL Ltd., Japan) at a voltage of 100 kV, equipped with a Mega view G2 camera. Samples for TEM experiments were prepared by spin-coating a drop of NPs in dichloromethane on a carbon-coated TEM grid.

Drug Loading Efficacy. The drug loading efficiency was evaluated by utilizing high-performance liquid chromatography (HPLC) with a Waters 2489 detector set to 303 nm, and the mobile phase specified in the calibration curve. Analyses were conducted on a known quantity of Methotrexate sodium (MTX) laden with copolymer.[15] The drug loading was calculated as the amount of drug (in milligrams) supplied per 100 mg of polymer, whereas the encapsulation efficiency was calculated as the ratio of drug encapsulated to the initial amount of drug used in the formulation.[16]

In Vitro Drug Release. To study the drug release profile of the synthesized MTX encapsulated iron oxide NPs modified with PLGA−PEG 400 copolymer, 3 mg of drug-encapsulated NPs were dispersed in 30 mL of phosphate-buffered solution (pH 7.4) and incubated at 37 °C.[17] At designated time intervals, a sample (3 mL) was withdrawn, and the same volume was reconstituted with a fresh phosphate-buffered solution and acetate buffer. The samples were analyzed by using HPLC at 303 nm to quantify the MTX content. Furthermore, regarding the effect of pH on drug release, the test was performed in an acidic acetate buffer solution (pH 8.5) and at a temperature of 40 °C.

In Vitro Cytotoxicity Studies. *Cell Culture.* The MCF-7 breast cancer cells[18] were procured from the National Centre for Cell Science (NCCS) located in Pune, India. The cells were cultured in Dulbecco's Modified Eagle's Medium (DMEM) supplemented with 10% fetal bovine serum (FBS) obtained from the American Type Culture Collection (ATCC) located in Mumbai, India. Subsequently, the cells underwent treatment with penicillin (10,000 units/mL), streptomycin (15 mg/mL), Amphotericin B (30 μg/mL), and L-glutamine (2 mM) under controlled conditions of temperature at 37 °C, humidity at 95%, and CO_2 concentration at 5% (using an HF90 160W device from Heal Force). The cells were supplemented with 10% heat-inactivated fetal bovine serum (FBS), 1% nonessential amino acid (NEAA), and 1% PASTE, which is a solution commonly utilized for fixing cells in culture for downstream applications such as microscopy, immunostaining, and protein extraction. Upon achieving 80% confluency, the cells were collected, subsequently placed in 96-well plates at a density of 10,000 cells per well, and utilized for an investigation of cell viability.

Cellular Apoptosis by Flow Cytometry. The MCF-7 cell lines[19] were initially cultured and subsequently exposed to the IC-50 concentration of the specimen. Following the cellular treatment, a double wash with cold Phosphate Buffer Solution was performed. Subsequently, the cells were suspended once again in 1X binding buffer, with a density of 1×10^6 cells/m. The land cells were segregated into distinct categories, namely, Unstained cells, Control group, Annexin only, PI only, and Treatment. The labeled tubes were supplemented with Annexin V FITC and PI. Following vortexing and incubation for 15 min at ambient temperature, 1X Binding buffer was

https://doi.org/10.1021/acsomega.3c03430
ACS Omega 2023, 8, 27634−27649

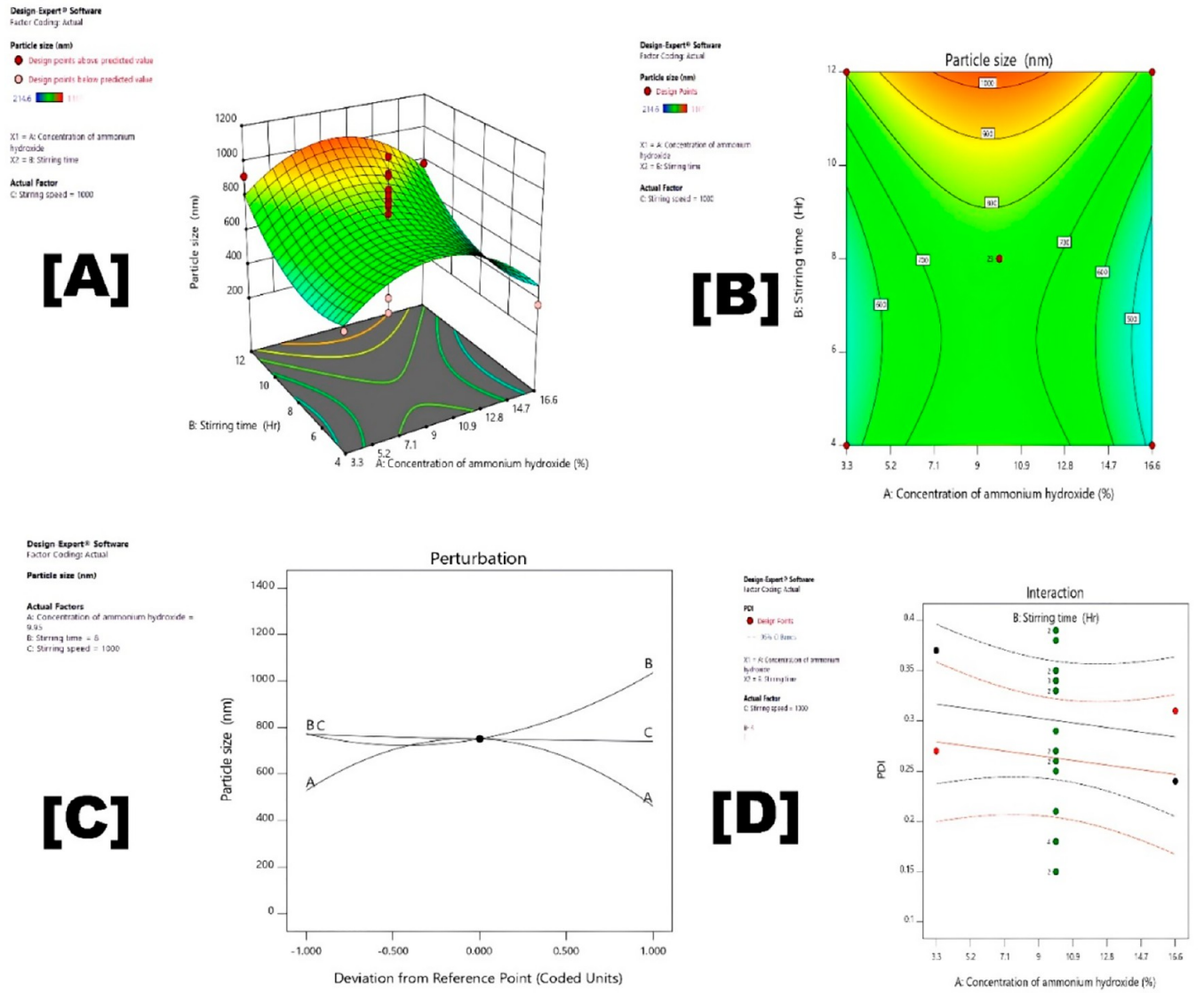

Figure 2. (A) Response surface plots play a significant role in the optimization of variables using experimental design, particularly in the context of Design of Experiments (DoE). These plots provide a visual representation of the relationship between the independent variables (factors) and the response variable in a multidimensional space. (B) Contour plots of particle size depict curves or lines that connect points of equal particle size across a two-dimensional space. These curves represent regions where the particle size is constant, allowing researchers to identify patterns and trends. (C) By examining the direction of the perturbations, it was identified that the factor (stirring time) has the biggest effect on the response variable, i.e., particle size. The larger the perturbation, the more significant the effect of the factor. Perturbation plots are important in DoE as they examine the impact of factors on a response variable. (D) Effect of ammonium hydroxide concentration and stirring time and their interaction on Y_1 at a fixed level of stirring speed.

introduced to each tube and subsequently subjected to analysis via the Flow Cytometer within a time frame of 1 h.

Cell Cycle Analysis. The exposure of MCF-7 cells to control, Methotrexate (MTX), and drug formulation for a duration of 24 h resulted in a concentration-dependent increase in the population of cells in the G0/G1 phase, accompanied by a subsequent reduction in the S phase.[20] The administration of drug formulation treatment resulted in a significant increase in the proportion of MCF-7 cells in the G0/G1 phase, with a recorded value of 53.2% as compared to the control group, which exhibited a value of 47.5%. The drug formulation treatment resulted in a reduction of the population of cells in the S phase from 20.6% in the control cultures to 15.1%.

In Vitro Cytotoxicity (MTT Assay). The MCF-7 breast cancer cells were cultured in 96-well plates at a density of 5×10^3 per well and were subjected to a 24 h incubation period. Subsequently, the cells underwent treatment with MTX that was dissolved in DMSO, as well as MTX-SPIONs that were administered in DMEM media supplemented with 10% FBS and antibiotics.[21] Following a 6 h incubation period, the transfection media was substituted with a novel Dulbecco's Modified Eagle's Medium (DMEM) solution supplemented with 10% fetal bovine serum (FBS) and antibiotics. Subsequent to the initial incubation, the cells underwent further incubation periods of 24, 48, and 72 h, respectively. Following this, the cells were subjected to viability assessment using the MTT assay. The relative percentage of cell viability in each treatment group was calculated with respect to the

https://doi.org/10.1021/acsomega.3c03430
ACS Omega 2023, 8, 27634−27649

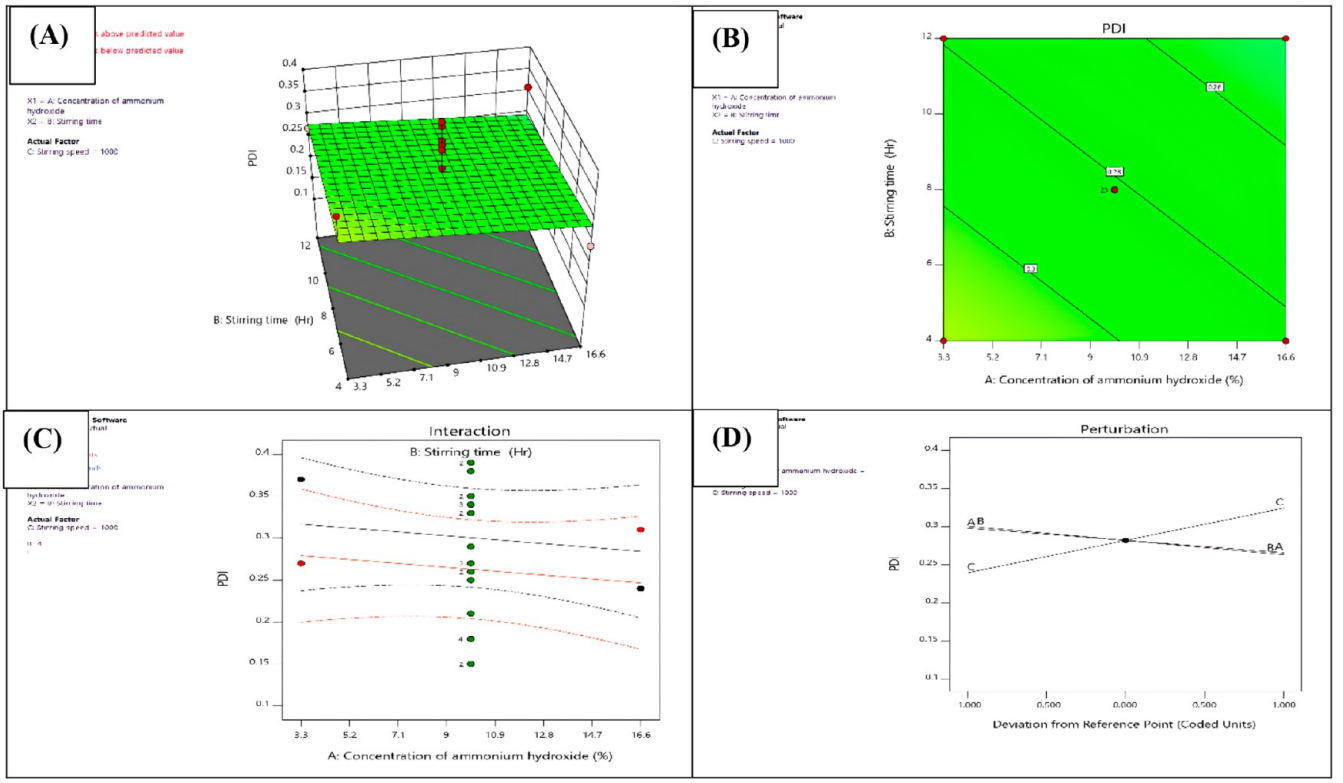

Figure 3. Effect of (A) ammonium hydroxide concentration and (B) stirring time in PDI with their interaction on Y_2 at a fixed level of stirring speed. (C) By examining direction of the perturbations, it was identified that the factor (stirring speed) has the biggest effect on the response variable, i.e., PDI. (D) The larger perturbation, the more significant the effect of the factor.

control cells. A one-way ANOVA was conducted to analyze the data, followed by Tukey's multiple comparison test to assess the significance of differences among the groups.

Mitochondrial Membrane Potential. The MCF-7 cells were cultured and subjected to treatment with the IC_{50} dose of both the standard and formulations. Following this, the cells were incubated for a duration of 24 h. Following incubation, the medium was extracted, and the cells were retrieved using trypsin EDTA.[22] The collected cells were then placed in a 1.5 mL tube and rinsed once with 500 μL of chilled PBS. Subsequently, the cellular pellets were distributed into 400 μL of JC-1 staining buffer containing 2 μM JC-1 dye, and the resultant samples were subjected to acquisition in a Flow Cytometer within a time frame of 60 min.

Reactive Oxygen Species. The MCF-7 cells were cultured and subjected to treatment with IC_{50} doses of the samples, followed by an incubation period of 24 h.[23] Following incubation, the medium was extracted, and the cells were collected through trypsin EDTA and subsequently gathered in a 1.5 mL tube. The cells were then rinsed once with 500 μL of chilled PBS. Subsequently, the cellular pellet was resuspended in 100 μL of phosphate-buffered saline (PBS) containing 2 μM of 2′,7′-dichlorodihydrofluorescein diacetate (DCFDA) and subjected to flow cytometry analysis within a time frame of 60 min.

Stability Study. Methotrexate-loaded SPIONs modified with PLGA−PEG copolymer were stored at 4 and 25 °C for a month. The MTX remaining in the polymer was determined at a particular time interval by using HPLC following the dissolution quantification and drug content.

Statistical Analysis. The data obtained were analyzed statistically. Descriptive statistics are presented as mean values ± standard deviation (SD). Moreover, the data represent the average ± standard deviation of 3 (n = 3) measurements.

RESULTS

Preformulation, Physical Appearance, and Calibration Curve of Methotrexate. The results of the preformulation study confirmed the purity and other allied properties such as color, odor, and texture of the tested MTX. The melting point results were observed between 195 and 210 °C, which is in compliance with Indian Pharmacopeia. The results of the solubility analysis indicated that MTX was freely soluble in sodium bicarbonate (28.5 mg/mL), chloroform (29.0 mg/mL), diethyl ether (32.0 mg/mL), and slightly soluble in water (4.0 mg/mL). The UV−vis spectrophotometer showed the absorption maxima at 303 nm, corresponding to standard MTX. Moreover, the HPLC calibration curve of MTX showed similar absorption at 303 nm with a retention time of 2.24 min and regression (r^2) of 0.985 (Figure 2B). The linearity was observed in the concentration range of 50 to 300 μg/mL (Figure 1C). The partition coefficient (log P) of MTX was observed as 0.8 ± 0.13. The partition coefficient measures drug lipophilicity, which indicates the ability to permeate the biological membrane.

Optimization of Variables Using Experimental Design. The initial trials revealed that the ammonium hydroxide concentration was 3.3−16.6% at low and high concentrations, respectively. The elucidation was carried out using response surface plots and contour plots (Figure 2A and B). The perturbation plot is a graphical instrument utilized in the

https://doi.org/10.1021/acsomega.3c03430
ACS Omega 2023, 8, 27634−27649

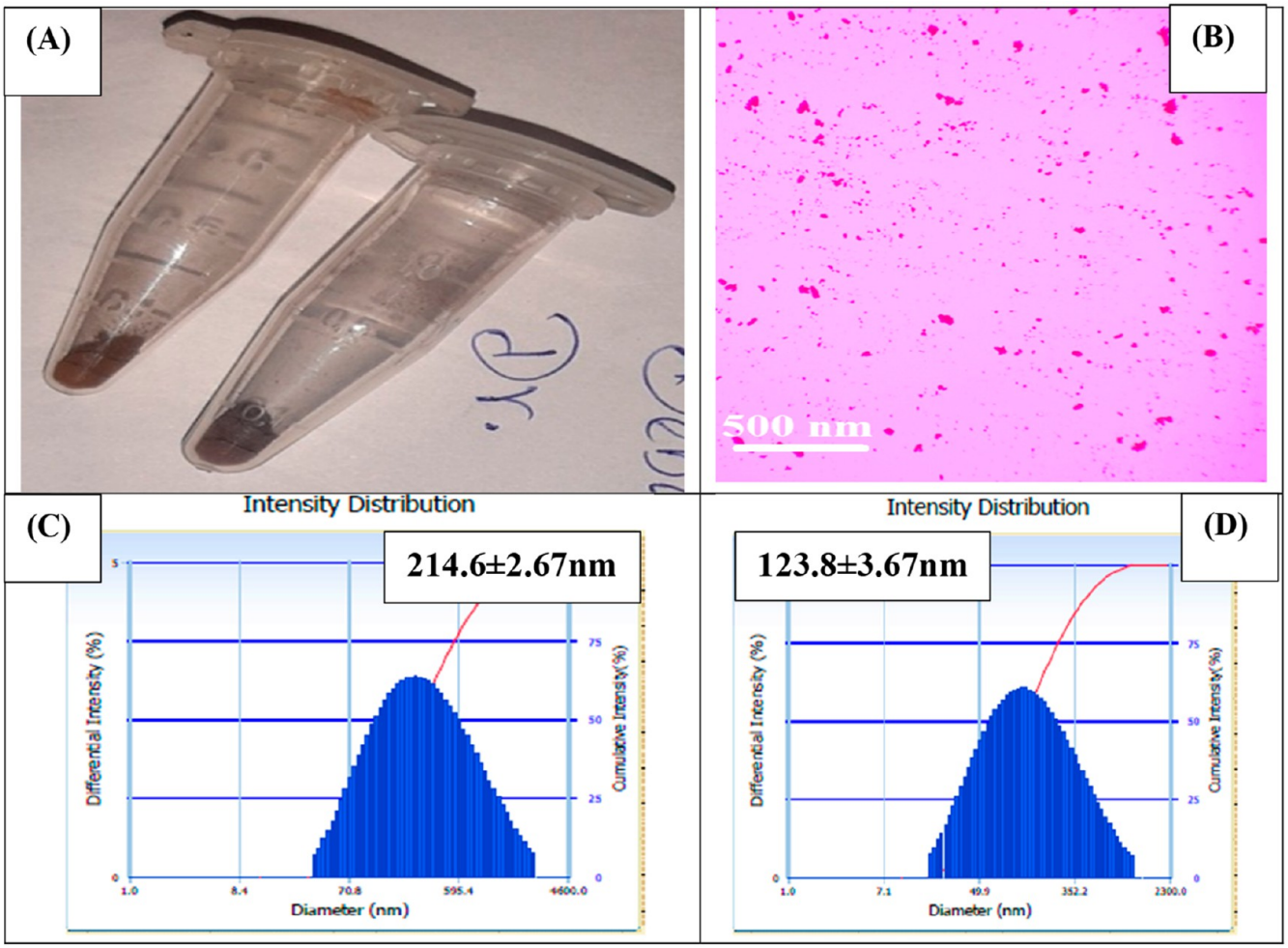

Figure 4. (A) Synthesized superparamagnetic iron oxide nanoparticles (SPIONs) that are produced through a chemical or physical process. These nanoparticles are often used in various biomedical applications, such as drug delivery, magnetic resonance imaging (MRI), and hyperthermia therapy, due to their unique magnetic properties. (B) Superparamagnetic iron oxide nanoparticles (SPIONs) visualized using fluorescence microscopy. (C) Particle size distribution of fabricated nanoparticles. (D) Particle size distribution of PLGA−PEG coated SPIONs.

Design of Experiments (DoE) to examine the impact of various factors on a response variable. Figure 2C is a form of scatter plot that depicts the correlation between the response variable and the various levels of each factor. The levels of the factors are illustrated through a sequence of perturbations or deviations from a central value.

The effects of the ammonium hydroxide concentration, stirring time, and their interaction on particle size (Y_1) at a fixed level of mixing speed are presented in Figure 2D. Further, Figure 3A and B shows in a form of a 3D surface plot and contour plot the effects of ammonium hydroxide concentration and stirring time and their interaction on PDI (Y_2) at a fixed level of mixing speed (Figure 3C). Furthermore, the analysis of perturbation patterns can aid in the identification of potential interactions among ammonium hydroxide concentration (A, %), Stirring time (B, h), and Stirring speed (C, RPM). If the perturbations for a given factor exhibit variability contingent on the level of another factor, it suggests the presence of an interaction between the two factors that warrants consideration, (Figure 3D).

$$Y_1\,(\text{nm}) = 751.94782608696 - 33.5125A + 131.3875B - 14.6C + 4.9AB + 75.825AC - 41.025BC - 257.12391304348A^2 + 152.77608695652B^2 + 4.4010869565215C^2 \quad (1)$$

The equation in terms of coded factors can be used to make predictions about the response for given levels of each factor. By default, the high levels of the factors are coded as +1, and the low levels are coded as −1. The coded equation is helpful in identifying the relative impacts of the factors by comparing the factor coefficients.

This mathematical model characterizes the relationship between the response variable and the input factors, which is represented by the final eq 1 in terms of coded factors in the context of Design of Experiments (DoE) optimization. The eq 1 was derived through the utilization of a regression model, which was fitted to the experimental data. The input factors were transformed into coded units to accommodate their varying scales and ranges.

The particle size at a fixed level of stirring speed can be represented in the form of coded factorial equation (eq 2).

$$Y_2 = +0.2817 - 0.0163A - 0.0188B + 0.0425C \quad (2)$$

https://doi.org/10.1021/acsomega.3c03430
ACS Omega 2023, 8, 27634−27649

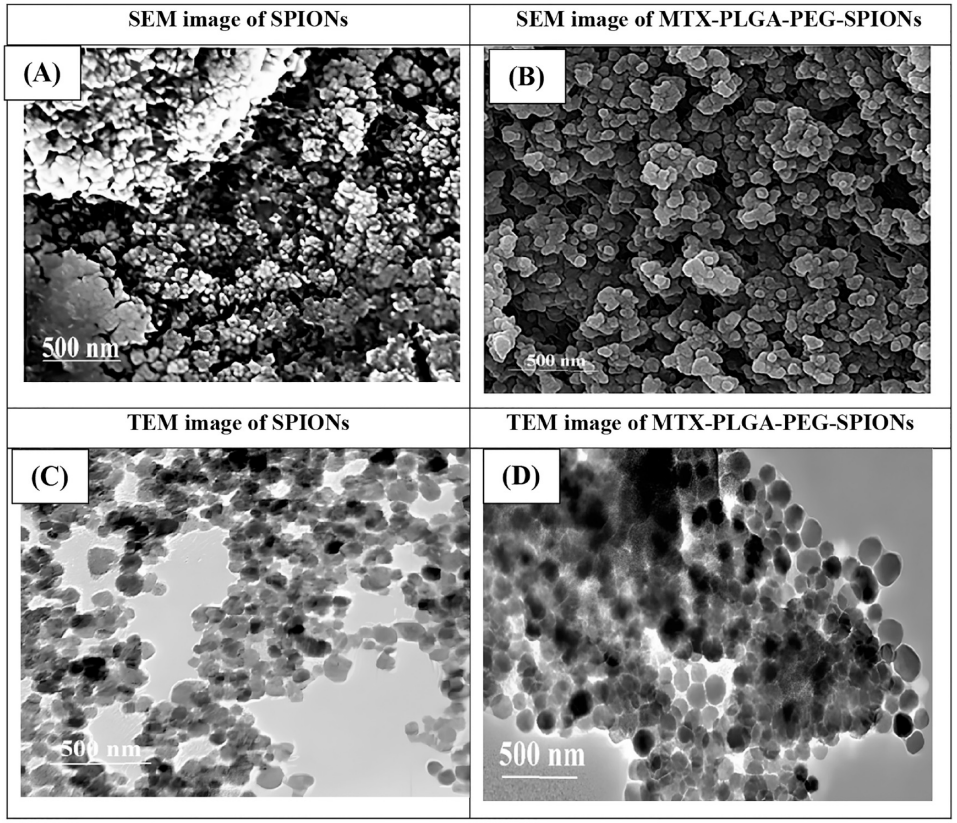

Figure 5. (A) Surface morphology of the SPIONs using scanning electron microscopy (SEM); SEM is crucial in analyzing the surface morphology of superparamagnetic iron oxide nanoparticles (SPIONs). (B) The PLGA−PEG coating over SPIONs enhances dispersibility and provides a smoother surface. SEM images show improved dispersion, reduced aggregation, and a more uniform size distribution, resulting in smaller particle sizes. (C) Transmission electron microscopy (TEM) of SPIONs; TEM is a valuable technique for examining the internal structure and morphology of SPIONs at high resolution. (D) PLGA−PEG coating over SPIONs in TEM images shows clearer visualization, uniform coating thickness, and smaller particle size. The coating process reduces aggregation and enables better dispersion, resulting in decreased particle size.

The eq 2 in terms of coded factors can be used to make predictions about the response for the given levels of each factor. By default, the high levels of the factors are coded as +1, and the low levels are coded as −1. The coded equation is useful for identifying the relative impact of the factors by comparing the factor coefficients. The equation in terms of actual factors can be used to make predictions about the response for given levels of each factor. Here, the levels should be specified in the original units for each factor. This eq 2 should not be used to determine the relative impact of each factor because the coefficients are scaled to accommodate the units of each factor, and the intercept is not at the center of the design space.

Fabrication of Superparamagnetic Nanoparticles. The concentration of ammonium hydroxide, stirring speed, and stirring time were optimized considering the particle size and PDI. However, the sodium hydroxide concentration was tested in the 3.3 to 16.6% range, with the starting time ranging from 4 to 12 h. Figure 4A and B shows both the synthesized superparamagnetic iron oxide nanoparticles (SPIONs) and their corresponding fluorescent microscopic images. After preliminary screening of data, the results indicated that 10% ammonium hydroxide at 800 rpm stirring speed for 12 h is the best suitable hydrodynamic particle size, and the size polydispersity of optimized nanoparticles was found to be 214.6 ± 2.67 nm and 0.280, respectively (Figure 4C).

Characterization of PLGAPEG-Coated Superparamagnetic Iron Oxide Nanoparticle. The hydrodynamic particle size and polydispersity of PLGA−PEG-coated SPIONs of MTX were observed as 123.8 ± 3.67 nm and 0.259, respectively (Figure 4D). Methotrexate (MTX) nanoparticles were found to be smaller after being coated on PLGA−PEG using superparamagnetic iron oxide nanoparticles (SPIONs). This reduction in particle size may be attributable to the compactness and denser packing of the SPIONs on the surface of PLGA−PEG, the fabrication method, or the interaction between MTX and the nanoparticles. Smaller particle sizes may occur from a denser packing pattern brought about by the presence of SPIONs. Supercritical liquid technology and emulsifying solvent volatilization are two examples of fabrication techniques that may have contributed to the miniaturization. In addition, MTX's interaction with nanoparticles may modify particle size by altering the conformation and packing of the polymer chains. Further research is required to fully understand the underlying mechanisms responsible for the observed decrease in particle size, and it is vital to keep in mind that these observations are specific to the experimental settings and formulation parameters utilized in this study. Moreover, the results of zeta potential indicated cationic change with a potential of 4.98 ± 1.56 mV. SEM images (Figure 5A) of SPIONs reveal their morphology, size, size distribution, surface texture, aggregation state, and internal structure. The images provide visual information about the

https://doi.org/10.1021/acsomega.3c03430
ACS Omega 2023, 8, 27634−27649

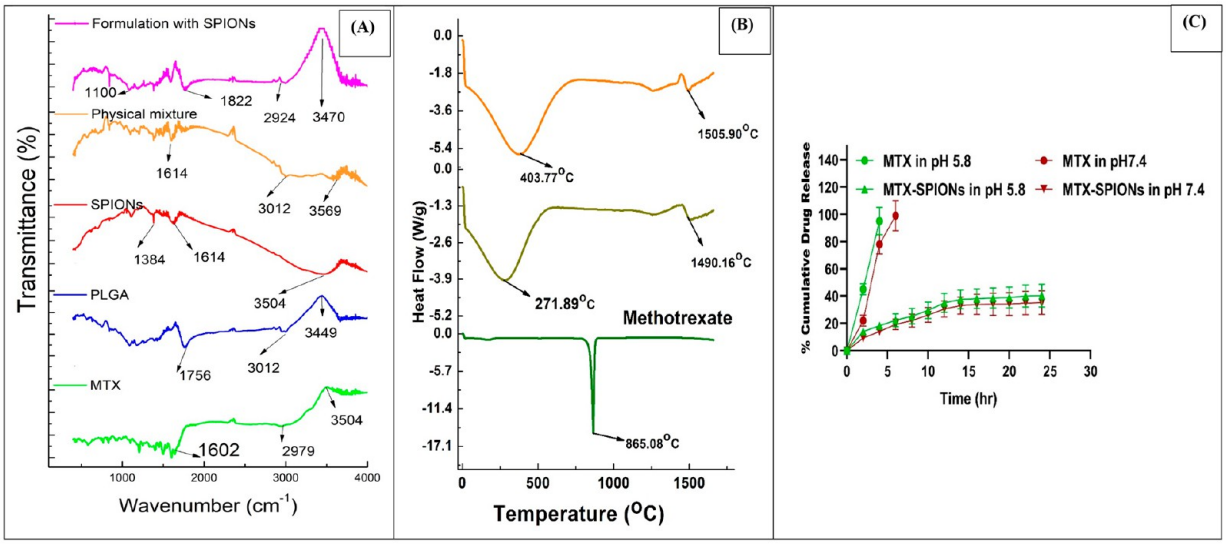

Figure 6. (A) Vibrational and structural analysis of MTX, PLGA, SPIONs, and physical mixture of optimized formulation composition. (B) DSC of MTX, PLGA, and physical mixture of optimized formulation composition. (C) In vitro release of methotrexate (MTX) and MTX-SPIONs at pH 5.8 and pH 7.4.

shape, size, and surface features of the nanoparticles, helping in understanding their physical properties and potential applications. In addition, the surface morphology image demonstrated that NPs were well aggregated, which might be due to the nanosized Fe_3O_4 SPIONs with PLGA−PEG copolymer and electrostatic repulsion force that develop steric hindrance between the copolymer chains on the encapsulated Fe_3O_4−NPs (Figure 5B). Further, the TEM image of uncoated SPIONs indicates that NPs are nanocrystalline, although their shape is primarily spherical with some hexagonal-shaped nanoparticles (Figure 5C). In TEM images of SPIONs after PLGA−PEG coating, several characteristic changes can be observed. The coating results in clearer visualization, uniform coating thickness, and smaller particle size. The reduced particle size can be attributed to conformal coating, improved dispersion, and reduced aggregation facilitated by the PLGA−PEG layer (Figure 5D). Furthermore, the average particle size was observed to be >500 nm, which corresponded well with the superparamagnetic size.

Compatibility Analysis. The results of the structural and functional interaction tested using FTIR are presented in Figure 6A. The FTIR spectrum of MTX showed prominent absorption bands at 3402 cm^{-1}, 1253 cm^{-1}, 1643 cm^{-1}, and 1516 cm^{-1}, attributed to O−H stretching, C−N stretching, C═O stretching, and C−H bending, confirming the purity of the drug. The FTIR spectrum of PLGA showed prominent absorption bands at 3012 cm^{-1} (C−H stretching) and 1756 cm^{-1} (C═O stretching). Additionally, the FTIR spectrum of SPIONs manifests prominent absorption bands between 3384 and 2073 cm^{-1}, which is the fingerprint region for iron oxide NPs. Most bands are O−H stretching/carboxylic acid and C≡C, characteristic of the inertial organic molecule present among the crystalline phase of SPIONs. Further, the FTIR spectrum of the physical mixture showed a minor shift in peaks compared to pure MTX. These shifts in peaks indicate intermolecular hydrogen bonds or some other weak forces, such as van der Waal forces or dipole moments among the polar functional groups of drug and polymer moieties. Furthermore, the pure drug exhibits a sharp endothermic melting peak at 865.08 °C, corroborated with the melting temperature of crystalline MTX. The DSC thermogram of PLGA showed a broad endothermic peak at 271.89 °C. The stability of the drug was suggested by the absence of melting endotherm of methotrexate at 865.08 °C in the DSC peak of the physical mixture of optimized formulation composition (Figure 6B).

Drug Content. The chromatography-based MTX encapsulation efficiency showed 46.8 ± 3.9% of MTX entrapment within SPIONs ($p > 0.05$), which was not affected by the coencapsulation of SPIONs. Moreover, the MTX loading was 2.8 mg/100 mg of polymer. Drug loading is crucial for formulations of drug delivery systems, because it directly affects the therapeutic dose available for the targeted tissue. Interestingly, the drug loading of NPs, formulated by an emulsion−diffusion−evaporation method using PVA as an emulsifier, was 4.5-fold higher than with the same method, described previously, using sodium cholate and 2.5-fold higher than with the nanoprecipitation technique (Danhier et al., 2009a). Moreover, the drug loading of nanoparticles was 2.8−4.8-fold higher than those described in previous studies.[24,25]

In Vitro Release Study. The in vitro release profiles for MTX were obtained by representing the percentage of MTX release with respect to the amount of MTX encapsulated within the polymer. The release study indicated that the MTX was released in two phases: an initial burst release, with a significant amount of drug released within 12 h, 35.1 ± 2.78%, followed by sustained release after 12 h (Figure 6C). The collective release profile over 2 days demonstrated 60.4% of MTX release was dependent on pH. The release profile study in varied pH showed that the release of MTX was modified and enhanced at pH 5.8. It is generally assumed that a drug is released by several processes, including distribution through the polymer matrix, release by polymer degradation, and solubilization and diffusion through microchannels that exist in the polymer matrix or are formed by erosion.

In Vitro Cytotoxicity Studies. *Apoptosis.* The apoptotic activity of three distinct groups, namely control, MTX, and MTX-SPIONs, was investigated through the utilization of flow cytometry. Upon conducting a comparative analysis of the cell count in relation to the control, it was observed that all three

https://doi.org/10.1021/acsomega.3c03430
ACS Omega 2023, 8, 27634−27649

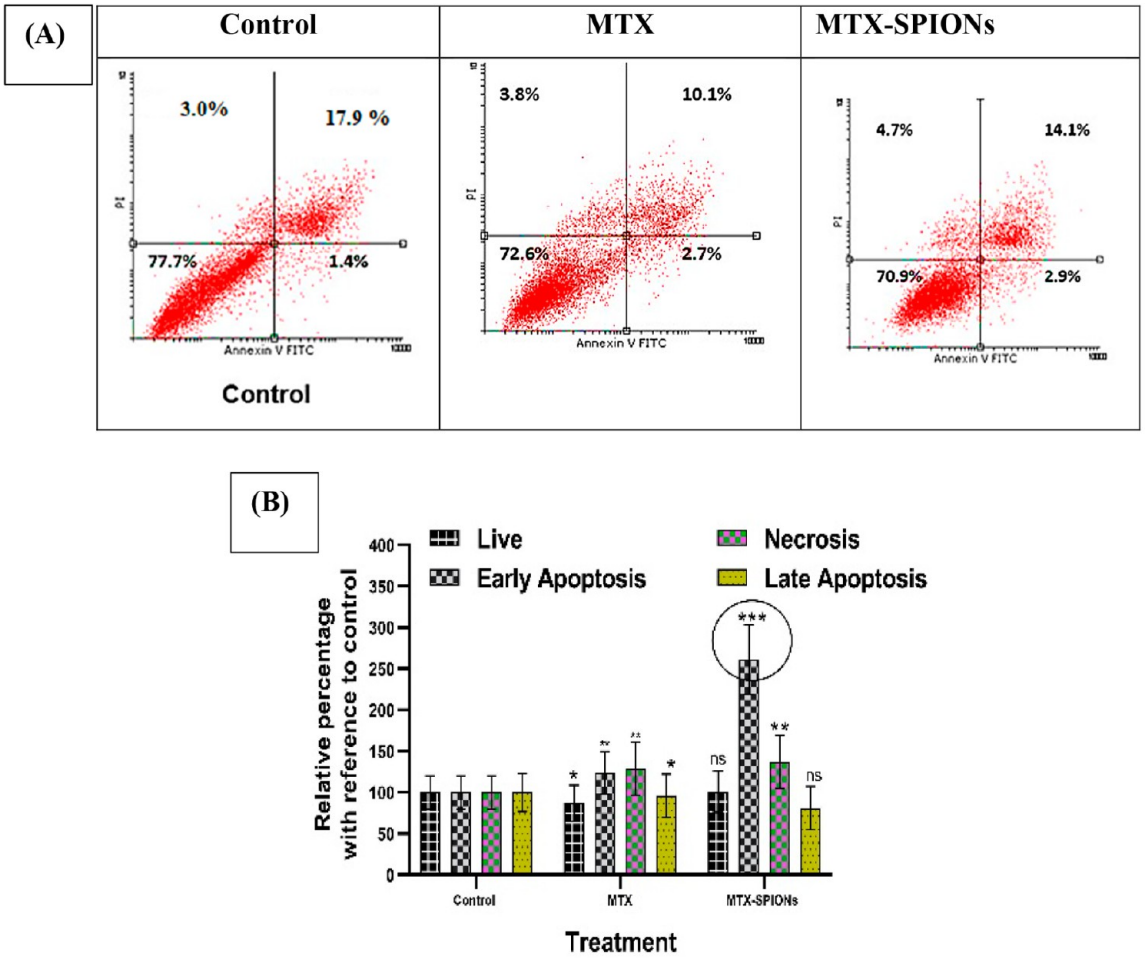

Figure 7. (A) The present study employs a scatter plot to visually represent the cellular apoptosis in three distinct experimental groups, namely Control, MTX, and MTX-SPIONs. (B). Bonferroni's one-way ANOVA test comparing cell inhibition between BOS and optimized BOS-CH-HSA-TPGS NPs across early apoptosis, live cells, late apoptosis, and necrosis (values are represented as mean ± SD (n = 3)) at 0.05 indicating significance (ns: $p > 0.05$; * $p < 0.05$; ** $p < 0.01$; *** $p < 0.001$).

formulations exhibited analogous quantities of viable cells. The MTX-SPIONs exhibit a statistically significant increase ($p < 0.0001$) in the proportion of cells in the early apoptotic stage, which is nearly twice as high as that observed in the control group and surpasses the levels observed in the pure drug. Both MTX and MTX-SPIONs exhibit a reduction in the number of cells in the late apoptotic phase relative to the control. The data presented in Figure 7A and B indicate a significant increase in the number of necrotic cells compared to the control group. The observations led to the conclusion that MTX-SPIONs exhibited a greater degree of apoptotic activity in comparison to both the control group and MTX. This phenomenon may be attributed to the heightened targeting efficacy and potential anticancer properties of the nanoparticles. In summary, it can be demonstrated that MTX-SPIONs exhibited noteworthy efficacy against cancerous cells via their apoptotic mechanism. The statistical analysis revealed $p < 0.0001$, indicating a significant outcome for the model.

Cell Cycle Analysis. The present study aimed to investigate the impact of control, MTX, and MTX-SPIONs on the cell cycle subsequent to a 24-h incubation period with their respective IC_{50} concentrations, utilizing flow cytometry as the analytical tool. The quantification of cells is contingent upon the quantification of DNA content as a percentage relative to the control within each respective phase. The results demonstrate a statistically significant increase in the percentage of cells in the G1 and G2 phases when treated with MTX-SPIONs compared to the control group ($p < 0.0021$). This finding suggests that the MTX-SPIONs formulation effectively decreases the metabolic activity necessary for cell division and impedes the organization of cellular contents. The administration of the unadulterated pharmaceutical agent triggers programmed cell death by interfering with the S phase of the cellular replication process. The statistical significance of the results for MTX and MTX-SPIONs, as depicted in Figure 8A and B, was demonstrated by the p-values obtained from Bonferroni ANOVA multiple comparison tests, which were 0.0218 and 0.0277, respectively. The present study reports the quantification of cells in G1, S, and G2 phases, denoting 52.3 ± 2.4%, 14.7 ± 1.56%, and 25.6 ± 2.31% for MTX, and 39.4 ± 3.67%, 11.4 ± 2.13%, and 41.5 ± 1.27% (mean ± SD) for MTX-SPIONs, respectively, in comparison to the control group.

In Vitro Cytotoxicity (MTT Assay). Based on our prior investigation, significant evidence exists to suggest that drug delivery utilizing SPIONs may enhance the cytotoxicity of chemotherapeutic agents. The determination of the therapeutic effectiveness of the drug (MTX) that is encapsulated in

https://doi.org/10.1021/acsomega.3c03430
ACS Omega 2023, 8, 27634−27649

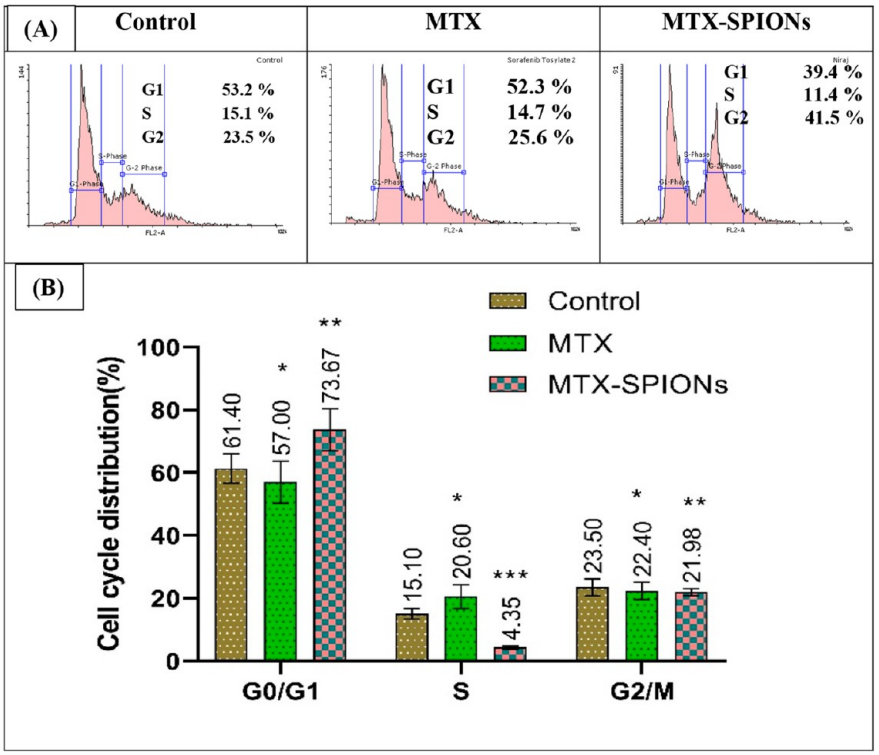

Figure 8. (A) Cell cycle analysis of control, MTX, and MTX-SPIONs. (B) Graphical representation of the cells presents in G1, S, and G2 phase using Dunet's One-way ANOVA test (values are represented as mean ± SD (n = 3)) at 0.05 indicating significance (ns: $p > 0.05$; * $p < 0.05$; ** $p < 0.01$; *** $p < 0.001$).

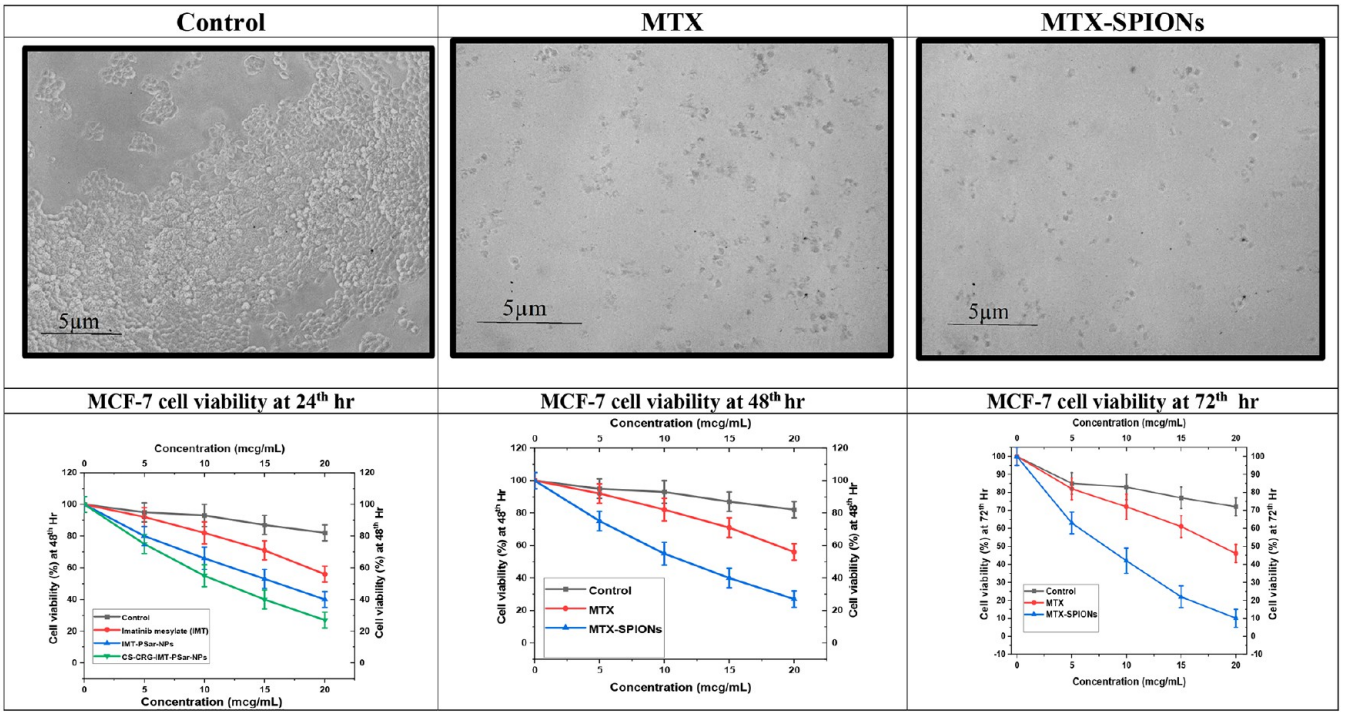

Figure 9. (A) Microscopic images of MCF-7 cells growth at 20 μg/mL with MTX, and MTX-SPIONs. (B) The growth curve in MCF-7 cells was determined by Trypan Blue (counting dye method), and the effects of exposure to MTX and MTX-SPIONs were evaluated at 0, 5, 10, 15, and 20 μg/mL concentrations after 24, 48, and 72 h and compared to control cells.

SPIONs is contingent on the uptake of nanoparticles and the subsequent release of the drug through internalized nanoparticles. The findings indicate that endocytosis must occur before drug release into the culture medium, as evidenced by the sustained release profile of MTX-SPIONs. The gradual increase in the MTX concentration when incubated with

https://doi.org/10.1021/acsomega.3c03430
ACS Omega 2023, 8, 27634−27649

MCF-7 cells is attributed to the sustained release profile of MTX-SPIONs. Figure 9 A and B displays microscopic images and growth curves of various treatments administered to MCF-7 cells. The MTT assay was employed to evaluate the impact of unbound MTX solution on cellular viability (%) in contrast to the impact of MTX-SPIONs, which encapsulate MTX, on cellular viability (%). The findings from the MTX assay demonstrate that MTX conjugated to SPIONs by which it exhibits prolonged antineoplastic activity against MCF-7 cell lines. After a duration of 72 h, it was determined that the MTX-SPIONs exhibit enhanced anticancer properties on MCF-7 cell lines in comparison to the control group. Table 2 presents the IC_{50} values for pure MTX and MTX-SPIONs at 24, 48, and 72 h. At the 24th hour of incubation, the IC_{50} values for MTX alone and MTX-SPIONs were determined to be 23.41 ± 3.60 μg/mL and 8.40 ± 0.36 μg/mL, respectively. Following a 72-h period, the IC_{50} values exhibited a decrease to 6.02 ± 0.70 μg/mL and 1.35 ± 0.30 μg/mL, respectively. The heightened intracellular drug concentrations and improved uptake efficiency are responsible for the superior anti-proliferative effect of SPIONs. The evaluation of cellular metabolic activity is of the utmost importance in determining cell viability. To this end, an MTT assay was conducted to evaluate the in vitro cytotoxicity and proliferation of MCF-7 cells. In vitro cytotoxicity investigations revealed that MTX-SPIONs exhibited superior cell growth inhibition compared to free MTX. The cytotoxicity of MTX, and CS-MTX-SPIONs against MCF-7 cells, was contingent upon both the duration and concentration of treatment.

Table 2. IC_{50} of Pure MTX and MTX-SPIONs after 24, 48, and 72 Hours on Cell Viability of MCF-7 Cell Line Using MTT Assay

Duration	Pure MTX (μg/mL)	MTX-SPIONs (μg/mL)
24 h	23.41 ± 3.60	8.40 ± 0.36
48 h	13.41 ± 1.11	4.20 ± 0.22
72 h	6.02 ± 0.70	1.35 ± 0.30

Mitochondrial Membrane Potential. The mitochondrial membrane potential (MMP) is generated by the uneven scattering of ions and protons on either side of the mitochondrial membrane. Reduced MMP levels may cause the opening of transition pores, resulting in mitochondrial permeability and the release of pro-apoptotic molecules. The mitochondrial matrix releases CytC into the cytosol, resulting in the activation of caspase-9, which initiates the mitochondrial apoptotic pathway. A decrease in MMP and ROS production is combined with a disturbance in oxidative phosphorylation, resulting in swelling and rupturing of the organelle. The

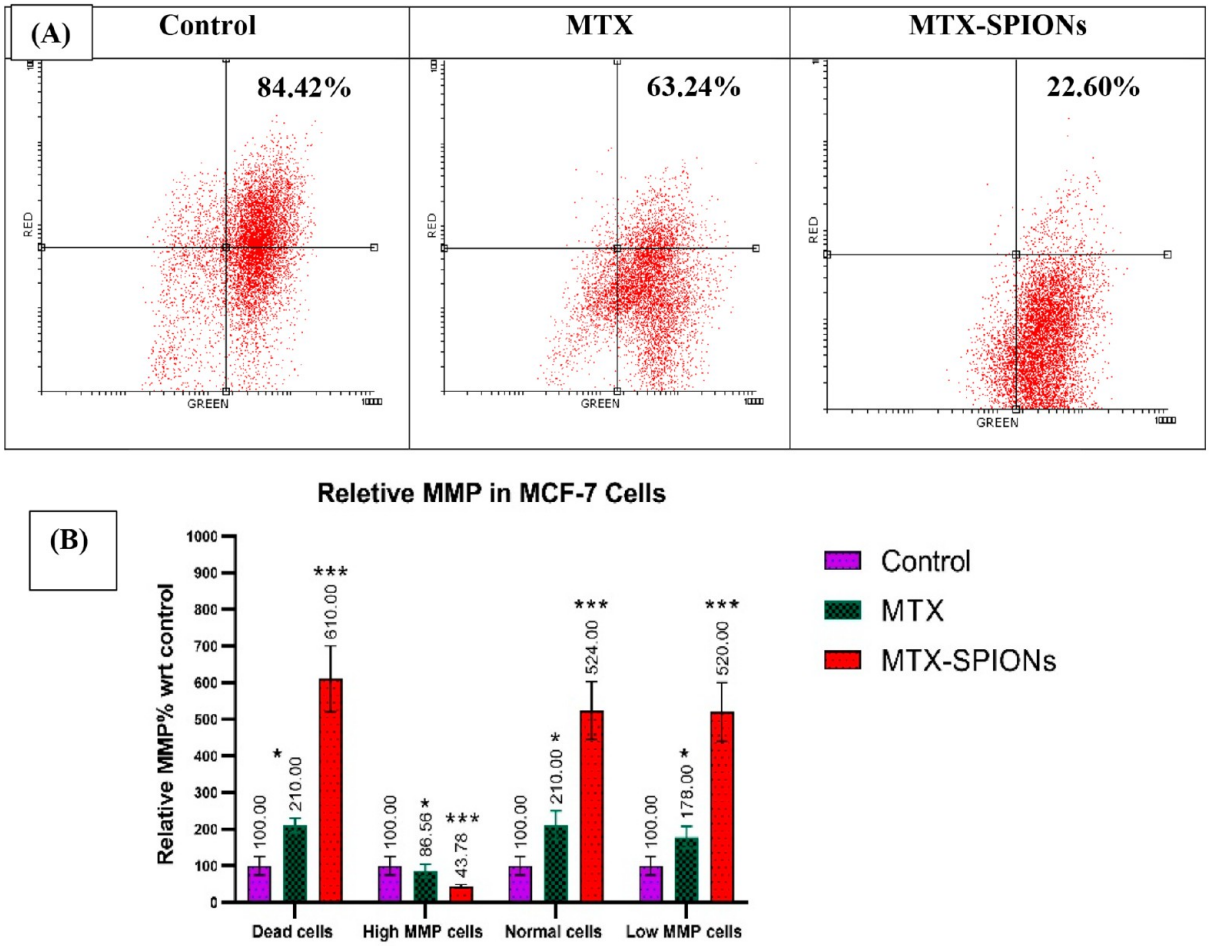

Figure 10. (A) MP detection by flow cytometry for control, MTX, MTX-SPIONs. (B) As per Bonferroni's multiple comparison test (values are represented as mean ± SD (n = 3)), determination of relative MMP%. * p < 0.01; ** p < 0.001; ** p < 0.0001 vs the control group; *** indicates high statistical significance (p < 0.0001) as compared with the control group.

https://doi.org/10.1021/acsomega.3c03430
ACS Omega 2023, 8, 27634−27649

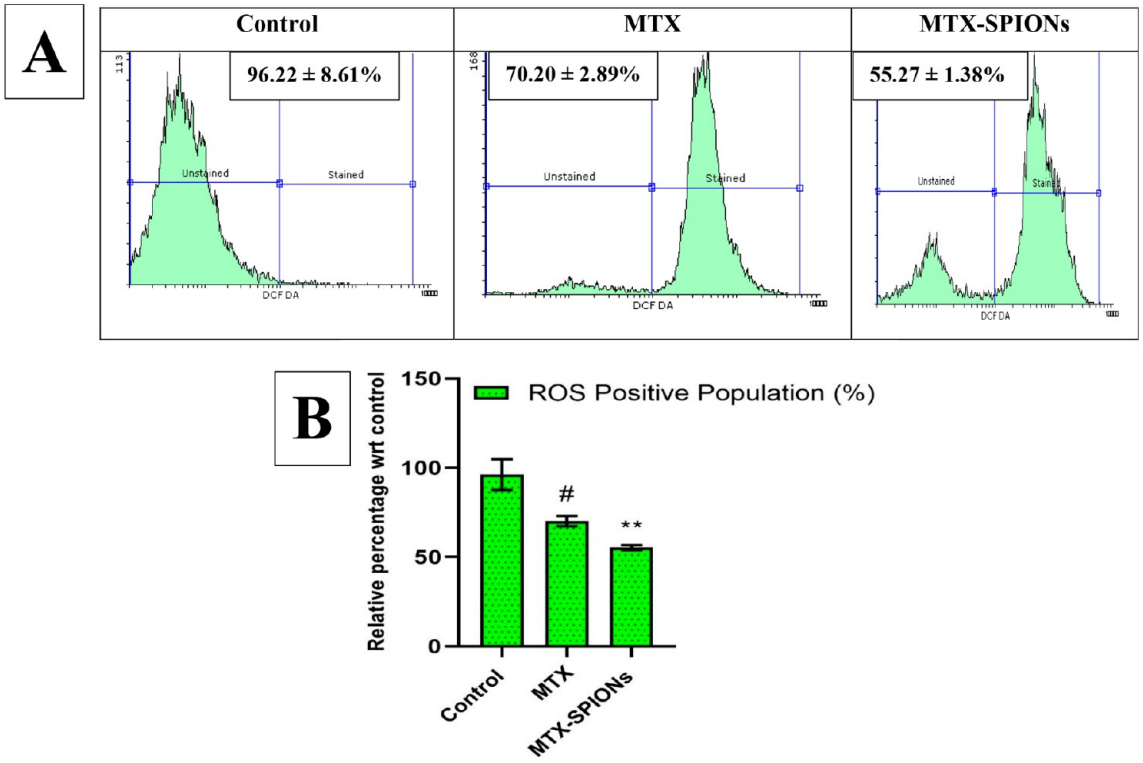

Figure 11. (A) MCF-7 cells were treated with MTX, MTX-SPIONs, and ROS-positive population percentage were calculated against the control group. (B) The cells were cultured, treated with IC_{50} doses of the samples, and incubated for 24 h. Data are expressed as mean ± SE of three independent experiments with similar results. ** $p < 0.01$; # $p > 0.05$.

Table 3. Stability Study of Optimized SPIONs at Different Storage Conditions

	4 ± 2 °C; 75 ± 5% RH		25 ± 2 °C; 40 ± 5% RH	
Time (days)	Drug content	Particle size (nm)	Drug content	Particle size (nm)
0	46.8 ± 3.9%	123.8 ± 3.67	46.7 ± 3.9%	123.8 ± 3.67
7	44.11 ± 1.23	123.7 ± 7.28	45.26 ± 1.55	124.45 ± 3.35
15	43.24 ± 1.11	122.28 ± 8.36	43.55 ± 1.37	228.68 ± 5.35
30	43.14 ± 0.15	125 ± 7.57	42.98 ± 0.9	254.2 ± 12.81

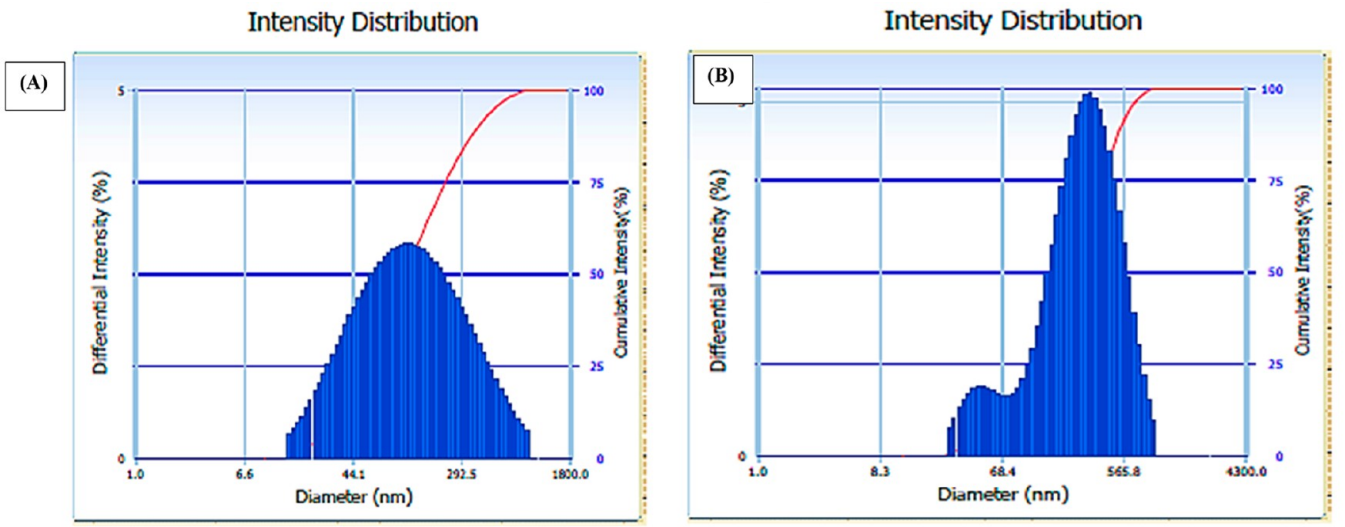

Figure 12. Particle size distribution of MTX-SPIONs at (A) 4 ± 2 °C; 75 ± 5% RH and at (B) 25 ± 2 °C; 40 ± 5% RH.

number of cells with High MMP with reference to the control was higher for the MTX (63.24 ± 3.89) than MTX-SPIONs formulations (22.60 ± 4.41) indicating that there are a smaller number of cells that are going into the apoptosis phase. There

https://doi.org/10.1021/acsomega.3c03430
ACS Omega 2023, 8, 27634−27649

are a greater number of cells in Low MMP of cells treated with MTX-SPIONs, indicating that the cells are leading their phase into apoptosis or necrosis as their mitochondrial function is disrupted, which is essential for the survival of cancer cells as shown in Figure 10A. The significant ($p < 0.0001$) effect of nanoparticles on mitochondria function was evaluated by one-way ANOVA Bonferroni's multiple comparison test (Figure 10B).

Reactive Oxygen Species. The analysis of ROS was conducted by using IC_{50} concentration of MTX and MTX-SPIONs exposure to MCF-7 cells. The ROS values are successfully established after 24 h. It can be observed from the graph that a significantly lower level of intracellular ROS (percentage-stained area) in MCF-7 ($p < 0.0001$) with reference to the control indicates the anticancer activity of the formulation. The percentage varied between MTX and MTX-SPIONs as 70.20 ± 2.89% and 55.27 ± 1.38%, respectively, as shown in (Figure 11A). Data were represented as mean ± SD. The results were evaluated to be statistically significant using one-way ANOVA Bonferroni's multiple comparisons tests, p-value was found to be $p < 0.0001$ (Figure 11B).

Stability Study. The results of the accelerated stability are presented in Table 3. After 30 days of study, the particle size distributions of the SPIONs were mentioned in Figure 12A and B. The results showed an insignificant variation in drug content and particle size measured using HPLC and zeta sizer, respectively. Therefore, these results suggested that MTX was stable during the tested period.

DISCUSSION

The objective of the study was to design and characterize a therapeutically effective nanoparticle delivery system for methotrexate loaded onto superparamagnetic iron oxide nanoparticles using poly(lactic-*co*-glycolic acid) and polyethylene glycol for the treatment of breast cancer. Results showed that the produced nanoparticles are spherical and aggregated at 500 nm in size, with an encapsulation effectiveness of 46.8 ± 3.9%. Intermolecular hydrogen bonding was shown to cause a shift in the major bands, as seen by Fourier-transform infrared spectroscopy, while the absence of a melting endotherm for MTX, as seen by differential scanning calorimetry, indicated total encapsulation with oxide nanoparticles. In vitro, release assays showed that the nanoparticles had a zeta potential of 4.98 mV and that following an initial burst release, the nanoparticles released a large amount (35.1 ± 2.78%) after 12 h.

The phenomenon of burst release in drug-loaded superparamagnetic iron oxide nanoparticles (SPIONs) can be attributed to a multitude of factors. In the initial stage of drug loading, there is a possibility of drug molecules adhering to the surface of the nanoparticle, resulting in an increased concentration of the drug that can be easily released upon exposure to the release medium. Insufficient encapsulation of the drug in SPIONs may lead to burst release, whereby areas with inadequate drug encapsulation or localization cause premature release during the initial phases. In addition, the aggregation of nanoparticles has the potential to generate specific areas with elevated drug concentrations, thereby promoting expedited drug release. In order to mitigate the issue of burst release, it is imperative to optimize the encapsulation process by modifying synthesis parameters. This approach can facilitate effective drug loading while simultaneously reducing the surface-associated drug. The implementation of surface modification techniques, such as the application of supplementary coating layers or alterations in surface chemistry, has the potential to enhance drug retention within nanoparticles. This can lead to a reduction in premature drug release and the attainment of a controlled and sustained release pattern. Furthermore, the integration of barrier layers or the utilization of controlled release mechanisms, such as multilayered or core−shell architectures, can effectively modulate drug release kinetics, thereby mitigating the occurrence of burst release and achieving a more protracted release profile. The stability study also showed that the medicine was stable with only a very little amount of encapsulated drug loss.

The folate receptor and reduced folate carrier are responsible for MTX internalization in tumor cells, and MTX has been intensively researched as a nanotheranostic drug for cancer treatment. The use of SPIONs as drug delivery vehicles is appealing due to SPIONs' biocompatibility and potential for biological applications. A supercritical liquid technique, which shows great promise, was used to make the drug−polymer magnetic composite nanoparticles in this study. The study concluded that the nanoparticles created had useful qualities for drug delivery to breast cancer cells. The medicine is protected from degradation, and bioavailability is increased thanks to the nanoparticles' high encapsulation efficiency and drug stability. The in vitro release study's findings of an explosive first release have further benefits, including the potential to accelerate the administration of a therapeutic dose. However, more study is needed to determine the sustained release profile and in vivo efficacy of the nanoparticles.

The optimal ammonium hydroxide content, stirring speed, and stirring time for nanoparticle synthesis were determined by using a Box−Behnken design. Using this layout, impact of each variable and their interactions on the outcome can be analyzed, leading to a more reliable and repeatable procedure. An HPLC calibration curve was used to determine the linearity of the drug concentration, which is crucial for estimating the drug concentration in the nanoparticles.

In terms of targeting breast cancer cells with drugs, the engineered nanoparticles show promise. The use of superparamagnetic iron oxide nanoparticles as carriers for drug delivery is a promising method because of their biocompatibility and potential biological uses. One promising method for the creation of such systems is the use of supercritical liquid technology in the production of drug−polymer magnetic composite nanoparticles.

The objective of the current investigation was also to examine the apoptotic activity and influence on the cell cycle of control, MTX, and MTX-SPIONs through the utilization of flow cytometry as an analytical instrument. The research revealed that MTX-SPIONs demonstrated significant effectiveness against malignant MCF-7 cells via their apoptotic pathway by triggering a programmed cell death. The findings indicate that the formulation of MTX-SPIONs successfully reduced the metabolic activity required for cell division and hindered the arrangement of intracellular components. In addition, the investigation presents an analysis of cell quantification in the G1, S, and G2 phases, revealing a noteworthy rise in the proportion of cells in the G1 and G2 phases upon exposure to MTX-SPIONs in comparison to that in the control cohort. The results indicate that the utilization of superparamagnetic iron oxide nanoparticles (SPIONs) for drug delivery may

https://doi.org/10.1021/acsomega.3c03430
ACS Omega 2023, 8, 27634−27649

augment the cytotoxicity of chemotherapeutic agents. The gradual increase in the MTX concentration observed upon incubation with MCF-7 cells was found to be responsible for the sustained release profile of MTX-SPIONs. This sustained release profile resulted in improved anticancer properties on MCF-7 cell lines as compared with the control group. The research findings suggest that the increased precision in targeting and potential anticancer characteristics of the nanoparticles could account for the amplified level of apoptotic activity that was detected with MTX-SPIONs. However, more study is needed to determine the sustained release profile and in vivo efficacy of the nanoparticles.

CONCLUSION

In the present study, superparamagnetic iron oxide nanoparticles (SPIONs) were synthesized by a coprecipitation process, and then the PLGA−PEG copolymer was used to encapsulate Fe_3O_4 NPs by an emulsion technique (w/o/w). The outcome shows that the copolymer chains successfully encapsulated the Fe_3O_4 NPs. These particles were employed in the encapsulation of methotrexate under mild conditions and could be used in drug delivery. Methotrexate encapsulation efficiency was 46.8 ± 3.9% for SPIO/MTX-NP, ($p > 0.05$), and methotrexate release occurred in two phases: an initial burst release exhibited a significant amount of drug released within 12 h (35.1% for Fe_3O_4 NPs modified with PLGA, PEG-400 nanoparticles), and after 12 h, the methotrexate release profiles showed a sustained release pattern. Our results suggest that supercritical liquid technology is a promising technique to produce drug−polymer magnetic composite nanoparticles for controlled-release drug systems. As a result, these nanoparticles could be suitable candidates for drug development. Further, the findings of this study illustrate the potential utility of SPIONs in facilitating the administration of chemotherapeutic agents for the treatment of breast cancer. The formulated MTX-SPIONs demonstrated noteworthy cytotoxicity against the malignant MCF-7 cells through the apoptotic pathway, resulting in the inhibition of cell division and the intracellular component arrangement. In addition, the protracted release kinetics exhibited by MTX-SPIONs were found to have enhanced their antineoplastic efficacy in comparison to that of the control cohort. The results indicate that the application of SPIONs in drug delivery may augment the cytotoxicity of chemotherapeutic agents and enhance the accuracy of cancer cell targeting. Additional research is required to evaluate the clinical utility of chemotherapeutic agents delivered via superparamagnetic iron oxide nanoparticles (SPIONs) for the treatment of breast cancer.

ASSOCIATED CONTENT

Data Availability Statement

Data will be made available on request.

AUTHOR INFORMATION

Corresponding Authors

Sankha Bhattacharya − *School of Pharmacy & Technology Management, SVKM'S NMIMS Deemed-to-be University, Shirpur, Maharashtra 425405, India;* orcid.org/0000-0002-0771-9582; Phone: +917878777207; Email: sankhabhatt@gmail.com

Nemat Ali − *Department of Pharmacology and Toxicology, College of Pharmacy, King Saud University, Riyadh 11451, Saudi Arabia*; Email: nali1@ksu.edu.sa

Authors

Bhupendra G Prajapati − *Shree S. K. Patel College of Pharmaceutical Education and Research, Ganpat University, Kherva 384012, India*

Mohamed Mohany − *Department of Pharmacology and Toxicology, College of Pharmacy, King Saud University, Riyadh 11451, Saudi Arabia*

Mourad A. M. Aboul-Soud − *Department of Clinical Laboratory Sciences, College of Applied Medical Sciences, King Saud University, Riyadh 11433, Saudi Arabia*

Rehan Khan − *Public Health Research Institute, Rutgers, New Jersey Medical School, Newark, New Jersey 07103, United States*

Complete contact information is available at: https://pubs.acs.org/10.1021/acsomega.3c03430

Author Contributions

The author declares that the work was done, analyzed, drafted by the author of this manuscript. The author had read and approved the final manuscript.

Notes

The authors declare no competing financial interest.

ACKNOWLEDGMENTS

This initiative would not have been possible without the help and support of Dr. R.S. Gaud, Pharma Section Director, SVKM's NMIMS Deemed-to-be University, Mumbai, India. Correspondingly, the authors would like to thank DIYA LAB, Mumbai, India, for its logistical and analytical assistance throughout the development of this project. This research was funded through the Researchers Supporting Project Number (RSPD2023R758), King Saud University, Riyadh, Saudi Arabia.

REFERENCES

(1) Shen, T.; Zhang, Y.; Zhou, S.; Lin, S.; Zhang, X.-B.; Zhu, G. Nucleic Acid Immunotherapeutics for Cancer. *ACS Applied Bio Materials* **2020**, *3* (5), 2838−2849.

(2) Li, Y.; Randriantsilefisoa, R.; Chen, J.; Cuellar-Camacho, J. L.; Liang, W.; Li, W. Matrix Stiffness Regulates Chemosensitivity, Stemness Characteristics, and Autophagy in Breast Cancer Cells. *ACS Applied Bio Materials* **2020**, *3* (7), 4474−4485.

(3) Chen, R.; Zhu, C.; Fan, Y.; Feng, W.; Wang, J.; Shang, E.; Zhou, Q.; Chen, Z. Polydopamine-Based Multifunctional Platform for Combined Photothermal Therapy, Chemotherapy, and Immunotherapy in Malignant Tumor Treatment. *ACS Applied Bio Materials* **2019**, *2* (2), 874−883.

(4) Liu, Y.; Gu, Y.; Fu, Z.; Xu, Y.; Wu, X.; Chen, J. T7-Functionalized Cationic Peptide as a Nanovehicle for Co-delivering Paclitaxel and siR-MeCP2 to Target Androgen-Dependent and Androgen Independent Prostate Cancer. *ACS Applied Bio Materials* **2021**, *4* (1), 807−819.

(5) Tezuka, K.; Umezawa, M.; Liu, T.-I.; Nomura, K.; Okubo, K.; Chiu, H.-C.; Kamimura, M.; Soga, K. Upconversion Luminescent Nanostructure with Ultrasmall Ceramic Nanoparticles Coupled with Rose Bengal for NIR-Induced Photodynamic Therapy. *ACS Applied Bio Materials* **2021**, *4* (5), 4462−4469.

(6) Spinozzi, E.; Ferrati, M.; Baldassarri, C.; Maggi, F.; Pavela, R.; Benelli, G.; Aguzzi, C.; Zeppa, L.; Cappellacci, L.; Palmieri, A.; et al. Synthesis of Carlina Oxide Analogues and Evaluation of Their Insecticidal Efficacy and Cytotoxicity. *J. Nat. Prod.* **2023**, *86*, 1307.

(7) Wang, J.; Zhang, J.; Wang, J.; Hu, X.; Ouyang, L.; Wang, Y. Small-Molecule Modulators Targeting Toll-like Receptors for Potential Anticancer Therapeutics. *J. Med. Chem.* **2023**, *66*, 6437.

(8) Halik, P. K.; Koźmiński, P.; Gniazdowska, E. Perspectives of Methotrexate-Based Radioagents for Application in Nuclear Medicine. *Mol. Pharmaceutics* **2021**, *18* (1), 33−43.
(9) Xing, R.; Li, S.; Zhang, N.; Shen, G.; Möhwald, H.; Yan, X. Self-Assembled Injectable Peptide Hydrogels Capable of Triggering Antitumor Immune Response. *Biomacromolecules* **2017**, *18* (11), 3514−3523.
(10) Mekseriwattana, W.; Thiangtrongjit, T.; Reamtong, O.; Wongtrakoongate, P.; Katewongsa, K. P. Proteomic Analysis Reveals Distinct Protein Corona Compositions of Citrate- and Riboflavin-Coated SPIONs. *ACS Omega* **2022**, *7* (42), 37589−37599.
(11) Singh, R.; Munya, V.; Are, V. N.; Nayak, D.; Chattopadhyay, S. A Biocompatible, pH-Sensitive, and Magnetically Separable Superparamagnetic Hydrogel Nanocomposite as an Efficient Platform for the Removal of Cationic Dyes in Wastewater Treatment. *ACS Omega* **2021**, *6* (36), 23139−23154.
(12) Rajendrakumar, S. K.; Uthaman, S.; Cho, C.-S.; Park, I.-K. Nanoparticle-Based Phototriggered Cancer Immunotherapy and Its Domino Effect in the Tumor Microenvironment. *Biomacromolecules* **2018**, *19* (6), 1869−1887.
(13) Liu, D.; Huang, C.; Wang, J.; Zhu, H.; Yao, P.; Liu, Z. Modeling and optimization of operating parameters for abrasive waterjet turning alumina ceramics using response surface methodology combined with Box−Behnken design. *Ceram. Int.* **2014**, *40* (6), 7899−7908.
(14) Mikelashvili, V.; Kekutia, S.; Markhulia, J.; Saneblidze, L.; Maisuradze, N.; Kriechbaum, M.; Almásy, L. Synthesis and Characterization of Citric Acid-Modified Iron Oxide Nanoparticles Prepared with Electrohydraulic Discharge Treatment. *Materials* **2023**, *16* (2), 746.
(15) Hsin, T.-H.; Dhenadhayalan, N.; Lin, K.-C. Ligusticum Striatum-Derived Carbon Dots as Nanocarriers to Deliver Methotrexate for Effective Therapy of Cancer Cells. *ACS Applied Bio Materials* **2020**, *3* (12), 8786−8794.
(16) Danhier, F.; Feron, O.; Préat, V. To exploit the tumor microenvironment: passive and active tumor targeting of nanocarriers for anti-cancer drug delivery. *Journal of controlled release* **2010**, *148* (2), 135−146.
(17) Volkov, V.; Sárria, M. P.; Gomes, A. C.; Cavaco-Paulo, A. Phosphorylated Silk Fibroin Matrix for Methotrexate Release. *Mol. Pharmaceutics* **2015**, *12* (1), 75−86.
(18) Talorete, T. P. N.; Isoda, H.; Maekawa, T. Agaricus blazei (Class Basidiomycotina) Aqueous Extract Enhances the Expression of c-Jun Protein in MCF7 Cells. *J. Agric. Food Chem.* **2002**, *50* (18), 5162−5166.
(19) Kuo, H.-P.; Chuang, T.-C.; Yeh, M.-H.; Hsu, S.-C.; Way, T.-D.; Chen, P.-Y.; Wang, S.-S.; Chang, Y.-H.; Kao, M.-C.; Liu, J.-Y. Growth Suppression of HER2-Overexpressing Breast Cancer Cells by Berberine via Modulation of the HER2/PI3K/Akt Signaling Pathway. *J. Agric. Food Chem.* **2011**, *59* (15), 8216−8224.
(20) Gao, Y.; Xie, M.; Yu, C.; Zhang, M.; Huang, J.; Li, Q.; Zhang, H.; Li, L. Heterologous Expression of Macrollins from Phytopathogenic Macrophomina phaseolina Revealed a Cytochrome P450 Mono-oxygenase in the Biosynthesis of β-Hydroxyl Tetramic Acid. *J. Agric. Food Chem.* **2021**, *69* (50), 15175−15183.
(21) Li, D.-D.; Yagüe, E.; Wang, L.-Y.; Dai, L.-L.; Yang, Z.-B.; Zhi, S.; Zhang, N.; Zhao, X.-M.; Hu, Y.-H. Novel Copper Complexes That Inhibit the Proteasome and Trigger Apoptosis in Triple-Negative Breast Cancer Cells. *ACS Med. Chem. Lett.* **2019**, *10* (9), 1328−1335.
(22) Yakkala, P. A.; Panda, S. R.; Naidu, V. G. M.; Shafi, S.; Kamal, A. Pyridine-Based 1,2,4-Triazolo-Tethered Indole Conjugates Potentially Affecting TNKS and PI3K in Colorectal Cancer. *ACS Med. Chem. Lett.* **2023**, *14* (3), 260−269.
(23) Beers, J. L.; Authement, A. K.; Isoherranen, N.; Jackson, K. D. Cytosolic Enzymes Generate Cannabinoid Metabolites 7-Carboxycannabidiol and 11-Nor-9-carboxytetrahydrocannabinol. *ACS Med. Chem. Lett.* **2023**, *14* (5), 614−620.
(24) Hu, J. J. Optical device and method for non-invasive real-time testing of blood sugar levels. WO2011034592A1, 2012.
(25) Singh, J.; Mishra, N. S.; Sharma, U.; Banerjee, S.; Sharma, Y. C. Comparative studies of physical characteristics of raw and modified sawdust for their use as adsorbents for removal of acid dye. *bioresources* **2011**, *6* (3), 2732−2743.

https://doi.org/10.1021/acsomega.3c03430
ACS Omega 2023, 8, 27634−27649